Acta Materialia 131 (2017) 271–279

Contents lists available at ScienceDirect

Acta Materialia

journal homepage: www.elsevier.com/locate/actamat

Full length article

Atomic-scale understanding of stress-induced phase transformation in cold-rolled Hf

Henglv Zhao [a], Min Song [a, **], Song Ni [a, *], Shuai Shao [b], Jian Wang [c], Xiaozhou Liao [d]

[a] State Key Laboratory of Powder Metallurgy, Central South University, Changsha, 410083, China
[b] Mechanical and Industrial Engineering, Louisiana State University, Baton Rouge, LA 70803, United States
[c] Mechanical and Materials Engineering, University of Nebraska-Lincoln, Lincoln, NE 68588, United States
[d] School of Aerospace, Mechanical and Mechatronic Engineering, The University of Sydney, Sydney, NSW 2006, Australia

ARTICLE INFO

Article history:
Received 13 August 2016
Received in revised form
4 March 2017
Accepted 19 March 2017
Available online 26 March 2017

Keywords:
Phase transformation
Dislocation source
Twinning

ABSTRACT

Identifying the character and the source of partial dislocations associated phase transformation from a hexagonal close-packed (HCP) structure to a face-centered cubic (FCC) structure is essential for understanding phase transformation mechanisms, but was rarely done using microscopy. Here, we report a stress-induced HCP to FCC phase transformation in pure hafnium during cold rolling. Detailed transmission electron microscopy investigations revealed that transformation-related partials stemmed from the dissociation of <a>-type dislocations. Successive gliding of partials on every other basal plane resulted in the orientation relationship between the two phases of $<11\bar{2}0>_{hcp}//<110>_{fcc}$, $<10\bar{1}0>_{hcp}//<\bar{1}12>_{fcc}$ and $[0001]_{hcp}//<111>_{fcc}$.Besides, a new way to form a twin relationship in the FCC structure was discovered.

1. Introduction

Solid-solid phase transformation in bulk materials has been one fundamental and long-standing research area, as the mechanical and physical properties of materials could change abruptly with structural transition [1–5]. Among different kinds of phase transformation, the transformation from a hexagonal close-packed (HCP) structure to a face-centered cubic (FCC) structure has been widely observed in metals and alloys, including Co [6,7], Co-32%Ni alloy [8,9], Ti [10,11], Ti-based alloys [12–14], stainless steel [1,2] and InAs nanowires [15]. Theoretically, the HCP to FCC phase transformation can be achieved through two approaches: Shockley partials glide on every other basal plane [1,2,6–9,12–15]; or shear-shuffle mechanisms through gliding two-layer disconnections or pure shuffle mechanisms through gliding four-layer disconnections on every other prism plane [11]. In the first approach, the transformation-related partials at the fronts of the FCC phase have Burgers vectors $\frac{a}{3}<1\bar{1}00>$ and their slip plane is the basal plane. The displays of these transformation-related partials have typically two scenarios: all the partials have the same Burgers vector; or they can have any one of the three Burgers vectors in the group of $\frac{a}{3}<1\bar{1}00>$ and hence are randomly arrayed. However, no consensus has been reached on which scenario is accounted for the HCP to FCC phase transformation, for there is still a lack of detailed and accurate atomic level identification for these transformation-related partials. Besides, it has not been clear on the sources of these partials.

Hafnium (Hf) has recently attracted increasing research interests due to its unique properties and significant applications in modern society [16–19]. For example, due to its large cross-section for thermal neutron capture and high corrosion resistance, Hf has been utilized as control rods in different types of nuclear reactors since late 1950s [19]. Pure Hf is of an HCP crystal structure (the α phase) at room temperature and a body-centered cubic (BCC) crystal structure (the β phase) at a temperature above 2016 K [16]. A phase transformation from the α phase to a simple hexagonal crystal structure (the ω phase) occurs under an applied pressure of 22 GPa–38 GPa [20–22]. High-energy ball milling on Hf powder leads to a transformation from the HCP phase to an FCC phase when the crystal size reaches several nanometers [23]. However, the HCP to FCC phase transformation has never been reported in bulk Hf. Moreover, the mechanism for HCP to FCC phase transformation is still unclear.

In the present study, we report the HCP to FCC phase

* Corresponding author.
** Corresponding author.
E-mail addresses: msong@csu.edu.cn (M. Song), song.ni@csu.edu.cn (S. Ni).

http://dx.doi.org/10.1016/j.actamat.2017.03.058
1359-6454/

transformation in cold-rolled bulk Hf processed at room temperature. Through comprehensive high-resolution transmission electron microscopy (TEM) investigation of FCC Hf lamellas in bulk Hf, the display of transformation-related partials was visualized successfully at the atomic level, and the source of these partials was deduced. Besides, we also discovered a new way for the formation of FCC twins in Hf.

2. Experimental procedure

The material used in this study was commercially pure Hf (99.99 wt%), purchased from Beijing General Research Institute of Nonferrous Metals. The as-received Hf plate exhibited equiaxed grains with an average size of ~20 μm. Small bars with dimensions of 30 mm × 10 mm × 3 mm were cut from the plate by spark machining. These small bars were annealed at the temperature of 1000 °C for 1 h and then were rolled at room temperature multiple times with a thickness reduction of 0.3 mm per pass to obtain deformed samples with a total thickness reduction of 60%. TEM specimens were cut from the transverse direction, mechanically ground to 50 μm, dimpled and then Ar^+ ion-milled using a Gatan 691 PIPS system with a voltage of 3 kV. For the initial and final milling, the ion incidence angle was set at 7° and 3°, respectively. TEM and high-resolution TEM investigations were performed using a FEI Titan G^2 60-300 Cs-corrected microscope operated at 300 kV.

3. Experimental results

3.1. HCP to FCC phase transformation in Hf

TEM and high-resolution TEM were used to identify the phase transformation in Hf. Fig. 1(a) shows a bright-field TEM image of the un-deformed hafnium. No lamella and few dislocations were seen in the un-deformed material. Fig. 1(b) shows a typical TEM image of cold-rolled samples with a thickness reduction of 60%.Lamellas with widths of up to tens of nanometers and lengths of several hundred nanometers formed in the cold-rolled material, as indicated by yellow arrows in Fig. 1(b). Fig. 1(c) presents a selected area electron diffraction (SAED) pattern obtained from the area in Fig. 1(b) that contains both the lamella structure and the matrix. The SAED pattern suggests that an HCP and an FCC structures co-exist in the selected area and the zone axis of the HCP and FCC structures presented in the pattern is $[1\bar{2}10]$ and [110], respectively. Dark-field imaging using FCC and HCP diffraction spots indicated that the lamellae are of the FCC structure while the matrix appears as the single HCP phase. The orientation relationship between the HCP and FCC phases is: $<11\bar{2}0>_{hcp}//<110>_{fcc}$ and $(0001)_{hcp}//\{111\}_{fcc}$. Fig. 1(d) presents a $[1\bar{2}10]_{hcp}$ and $[110]_{fcc}$ high-resolution TEM image showing the interface between an FCC lamella and the HCP matrix, further confirming the orientation relationship. Based on the orientation relationship and the crystallography of the two structures, it is expected to have $<10\bar{1}0>_{hcp}//<\bar{1}12>_{fcc}$(see the Supplementary Material Fig. S1). Interestingly, a high density of dislocations exists in the FCC lamellas. Some dislocation cores are indicated using white "T" in Fig. 1(d). The Burgers vectors of most dislocations in the FCC phase have a directional component parallel to the c-axis ([0001]) of the HCP matrix, implying that these dislocations accommodate the c-axis strain and thereby the introduction of the FCC lamellas may enhance the deformability of the material.

Based on the orientation relationship of the two phases, Fig. 2 depicts a possible mechanism of the phase transformation, in which the lattice parameters were measured from high-resolution TEM images: Shockley partial dislocations with Burgers vectors of the $\frac{a}{3}<10\bar{1}0>$ type were generated and glided on every other (0001) plane during rolling deformation. The dashed line in Fig. 2(a) presents a partial dislocation gliding on a(0001) habit plane. The following discussion assumes 5 Shockley partials emitted on atomic layers 1, 2, 3, 4, 5, respectively. The original atomic stacking sequence in the HCP matrix is … ABABABABAB …. Slip of the partial on layer 1 (a B stacking plane) results in a new stacking sequence of … ACBCBCBCBC … (the column "Step 1"). As the remaining steps go on, the final stacking sequence of … ACBACBACBA … (the column "Step 6") forms and a ten-layer FCC structure is created. This transformation process indicates that coordinated activation of $\frac{a}{3}<10\bar{1}0>$ partials gliding on every other(0001) plane gradually converts the HCP structure to the FCC structure. The model described in Fig. 2 leads to the orientation relationship obtained from the SAED and high-resolution TEM data shown in Fig. 1(c) and (d). Fig. 2(b) shows the lattice parameters and the orientation relationship of the two phases. The lattice parameters with error bars are measured in high-resolution TEM images. It shows that when the HCP structure transformed to the FCC structure, the lattice expansion amounted to +1.81%, and +6.06% along the$[10\bar{1}0]$, and[0001] directions, respectively.

Note that three different $\frac{a}{3}<10\bar{1}0>$ partial dislocations gliding on the basal plane with the angle 120° between each other would produce exactly the same stacking fault despite of the difference in the gliding directions. The atomic illustration is shown in the left bottom of Fig. 3. The solid circles in the figure represent the atoms of HCP phase, while the hollow circles indicate the atom positions after Shockley partial dislocations gliding on every other (0001) plane, converting the HCP stacking sequence to FCC stacking sequence. Though a coordinated sliding on every other (0001) plane is required for the HCP to FCC transformation, there is no restriction to the activation of any of the three $\frac{a}{3}<10\bar{1}0>$ dislocations on each (0001) plane. Fig. 3 shows there exists two scenarios for the HCP to FCC transformation—scenario A: all Shockley partial dislocations that contribute to the transformation have the same Burgers vector or gliding direction. This collectively produces a net macroscopic strain [24–26]; and scenario B: Burgers vectors are randomly selected, which leads to much smaller or even zero net macroscopic strain [27,28]. While both scenarios result in the HCP to FCC transformation, the net macroscopic strains introduced by the two types of transformation are different.

Fig. 4 shows two typical high-resolution TEM images of the HCP/FCC interfacial regions. The stacking sequence of the HCP phase is … ABABAB …, while the stacking sequence of the FCC phase is … ABCABC …, as shown in Fig. 2. In the transitional zone, several adjacent Burgers circuits based on the HCP lattice were drawn. Both 30°and 90°Shockley partial dislocations were observed (the identification of partial dislocations is shown in the Supplementary Material Fig. S2), and this is also the case for many other interfacial regions, indicating that scenario B is favored in this study.

3.2. The sources of phase transformation—related partials

Hf belongs to the IVb group in the periodic table, having a c/a ratio of 1.581 that is smaller than the ideal value of 1.633. During a deformation process of Hf, strain can be accommodated through slips and twinning [29,30]. Typically, Shockley partial dislocations can form in two ways: nucleation from special positions, which include the boundaries of nanocrystalline grains [7,27,31], free surface [15,31]and crack tips [32,33], and dissociation of full dislocations [34,35]. As the grain sizes of the Hf were much larger than the critical grain size needed for partial dislocation emission from grain boundaries [31,36], no grain boundary source was available. For most grains in the bulk coarse-grained Hf, there was also no free surface or crack tip. Therefore, the phase transformation—related partials formed only via the dissociation of full dislocations.

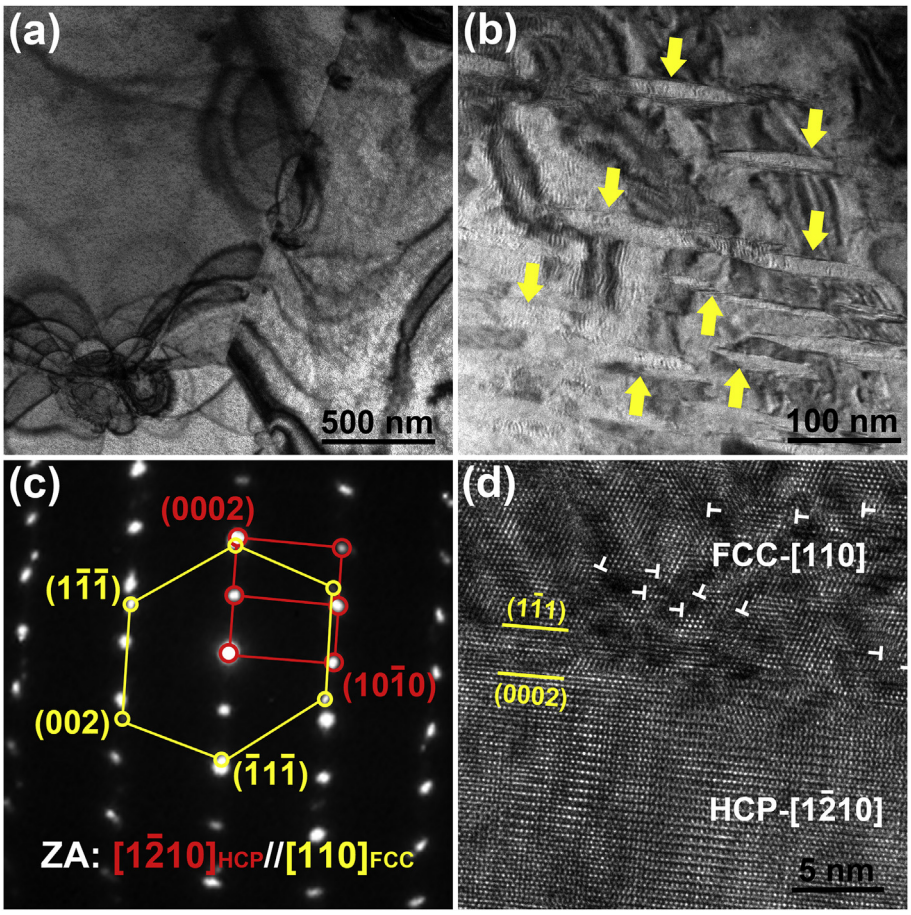

Fig. 1. (a) A bright-field TEM image of the un-deformed hafnium. (b) A bright-field image of the rolled specimen with numerous lamellas, indicated by yellow arrows. (c) The SAED pattern obtained both the lamella structure and the matrix in (b). (d) A high-resolution TEM image of an area with the HCP and FCC phases. The image was taken along the$[1\bar{2}10]_{hcp}$ and$[110]_{fcc}$ directions. (For interpretation of the references to colour in this figure legend, the reader is referred to the web version of this article.)

Shockley partial dislocations can typically stem from two possible sources: dissociations of <a>-type dislocations or dissociations of <a+c>-type dislocations. Regarding dissociation of <a> dislocation, there are two mechanisms. A: $1/3<11\bar{2}0>$(60° full dislocation) → $1/3<10\bar{1}0>$(30° partial) + $1/3<01\bar{1}0>$(90° partial), or B: $1/3<11\bar{2}0>$(screw dislocation) → $1/3<10\bar{1}0>$(30° partial) + $1/3<01\bar{1}0>$(30° partial). In this case, both ends of the FCC lamellas contain Shockley partials. In hafnium, <a>-type dislocations can slip on prism planes, basal planes [37]. Regardless of which plane they originally slip on,<a>-type dislocations dissociate on the basal plane. The only difference is that if <a>-type dislocations originally slip on the prism plane or the pyramidal plane, they should cross slip onto the basal plane first and then dissociate. The other possible source is dissociations of <a+c>-type dislocations. This situation is more complicated due to different dislocation geometries on different pyramidal planes: there are two kinds of <a+c>-type dislocations [38,39]. One is $\{01\bar{1}1\}$<a+c>-type dislocations. In the dissociation process, this kind of <a+c> dislocations dissociated firstly in the pyramidal plane as C:$1/3<11\bar{2}3>$(57.7° full dislocation) → $<0001>$(edge dislocation)+ $1/3<11\bar{2}0>$(screw dislocation), the dislocation with Burgers vector $1/3<11\bar{2}0>$ cross-slipped from the pyramidal plane to basal plane and then dissociated as $1/3<11\bar{2}0>$ → $1/3<01\bar{1}0>$+$1/3<10\bar{1}0>$. The other is $\{11\bar{2}2\}$<a+c>-type dislocations. This kind of <a+c> dislocations dissociated first in pyramidal planes as D: $1/3<11\bar{2}3>$(62.4° full dislocation) → $1/3<10\bar{1}3>$(80.1° dislocation)+$1/3<01\bar{1}0>$(screw partial), then the dislocation with Burgers vector $1/3<01\bar{1}0>$ cross-slipped from the pyramidal plane to the basal plane. Nevertheless, the residual dislocations associated with the two dissociations are all sessile as their Burgers vectors are not parallel to their slip planes. Thus, if these transformation-related partials come from the dissociation of <a+c> dislocations, at one end of the FCC band there must be many sessile dislocations. Furthermore, we calculated the energy change for those dislocation dissociations mentioned above (see Supplementary material Data S1). The dissociation of <a> (60° full dislocation) is the most energetically favorable among those dislocation dissociations.

In order to figure out the exact source of transformation-involved partials, we conduct high-resolution TEM observations at the two ends of many FCC lamellas. Fig. 5(a) shows the high-resolution TEM image of a whole FCC lamella with length of ~50 nm. Fig. 5(b) and (c) present the Fourier-filtered images of the white rectangular areas of the left and right ends of the lamella, respectively. The atomic stacking sequences in the left and right regions in Fig. 5(b) is … ABAB … (the HCP structure) and … ABCABC … (the FCC structure), respectively. Two Burgers circuits based on the HCP lattice were drawn in the transitional zone between the HCP and FCC structures, indicating one 30° and one 90° Shockley partial dislocations on two(0001) planes. Fig. 5(c) shows the right end of this FCC lamella, two Burgers circuits based on the HCP lattice were drawn, showing two 30° Shockley partial dislocations. Note that the red lines in Fig. 5(b) and (c) represent the same atom row in this FCC lamella. There is no sessile dislocation gathering at

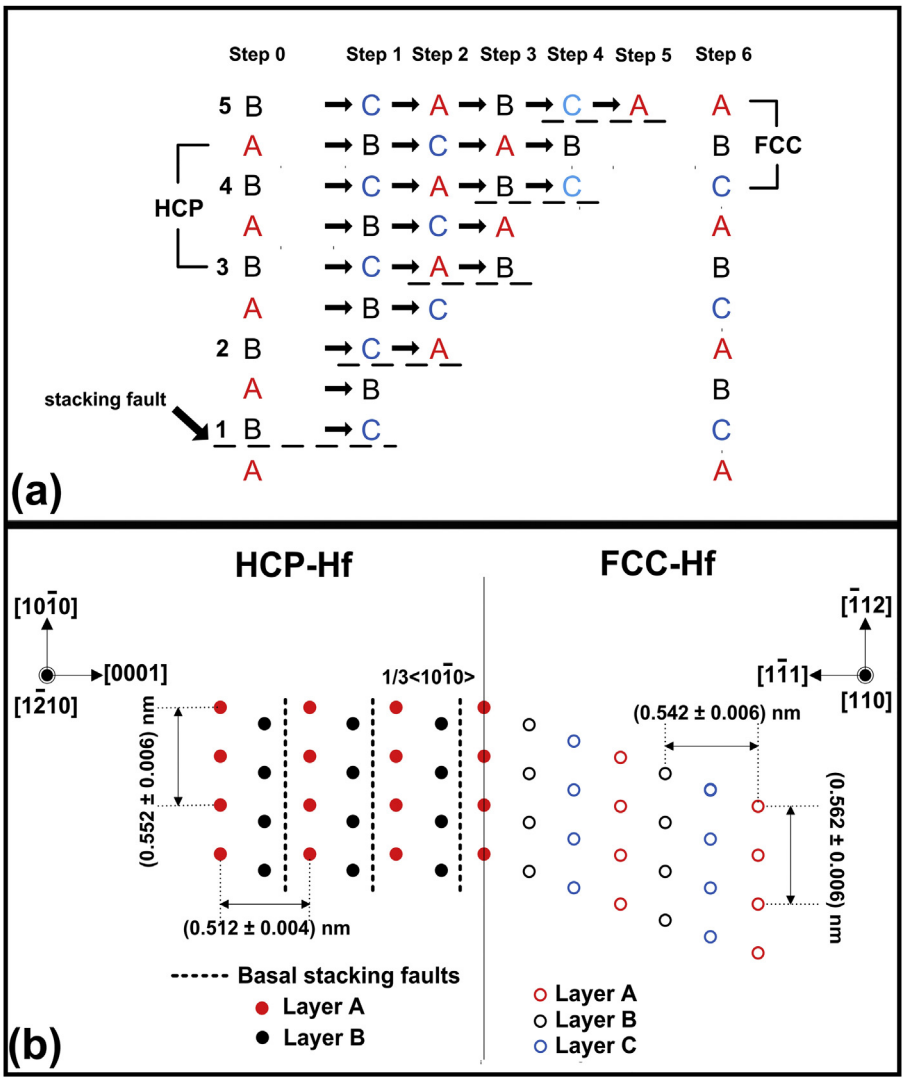

Fig. 2. Schematic illustration of the mechanism of HCP to FCC transformation. (a) Five partials gliding on planes represented by dash lines, creating a ten-layer FCC sequence. (b) Lattice parameters and the orientation relationship between the HCP and FCC phases.

the two ends of the FCC lamella, suggesting that the Shockley partials came from the dissociation of <a>-type dislocations. And this is also the case for many other lamellas. We also have conducted the contrast analysis with two-beam condition (see Supplementary Material Fig. S3) showing that in the deformation process, <a>-type dislocations were largely generated in HCP matrix and thus provide a sufficient dislocation source for these transformation-related partials. Moreover, atomic scale observation on FCC layers with length of less than 5 nm further confirms the dissociation of <a>-type dislocations. Fig. 5(d) shows the dissociation of a screw <a>-type dislocation on basal plane observed near another FCC lamella. It can be seen that two 30° Shockley partial dislocations glide on the basal plane, translating part of the HCP matrix into the FCC structure. The dissociation of a screw <a>-type dislocation leads to two 30° Shockley partial dislocations having opposite edge components on the basal plane [34]. Under the applied stress, two 30° partial dislocation would glide along the opposite direction due to having opposite edge components, which may shrink or extend the stacking faults and concomitant FCC structure. Fig. 5(e) shows the dissociation of a 60° mixed <a>-type dislocation resulting in a 30° partial and a 90° partial [35]. Thus, the partial dislocations indicated in Fig. 5(b) and (c) might be dissociated from screw dislocations and 60° mixed-type dislocations. The 90° pure edge partials dissociated from 60° mixed-type dislocations would be attracted by 30° partials at upper/lower layers of the same side due to attractive interaction resulted from the opposite edge components [15] and to release strains introduced by the accumulation of 30° partials, and then lead to the partials display in the interfacial regions between HCP and FCC in Fig. 4.

In the earlier discussion, we depicted that when the HCP structure transformed to the FCC structure, the lattice expansion amounted to +1.81%, along the[10$\bar{1}$0] directions, then there is a lattice mismatch strain of 1.81% between $\{0001\}_{hcp}$ and$\{111\}_{fcc}$. There should be a misfit dislocation with the Burgers vector $b = [11\bar{2}\,0]_{hcp}$ presented on every 55th $(10\bar{1}0)$ along the $[10\bar{1}0]$ direction in the $(0001)_{hcp}$ plane generated to release the lattice mismatch strain. Fig. 6 shows the existence of these misfit dislocations. The misfit dislocation is one of the sources for 60° mixed-type dislocations. The dissociation of them can expand the FCC phase along the width direction and then thicken the FCC lamellas.

Electron beam irradiation would lead to beam heating and knock-on displacement of TEM specimens [40,41]. As the electron beam dose was kept at a level of ~2×10^5 e $nm^{-2}s^{-1}$ during our

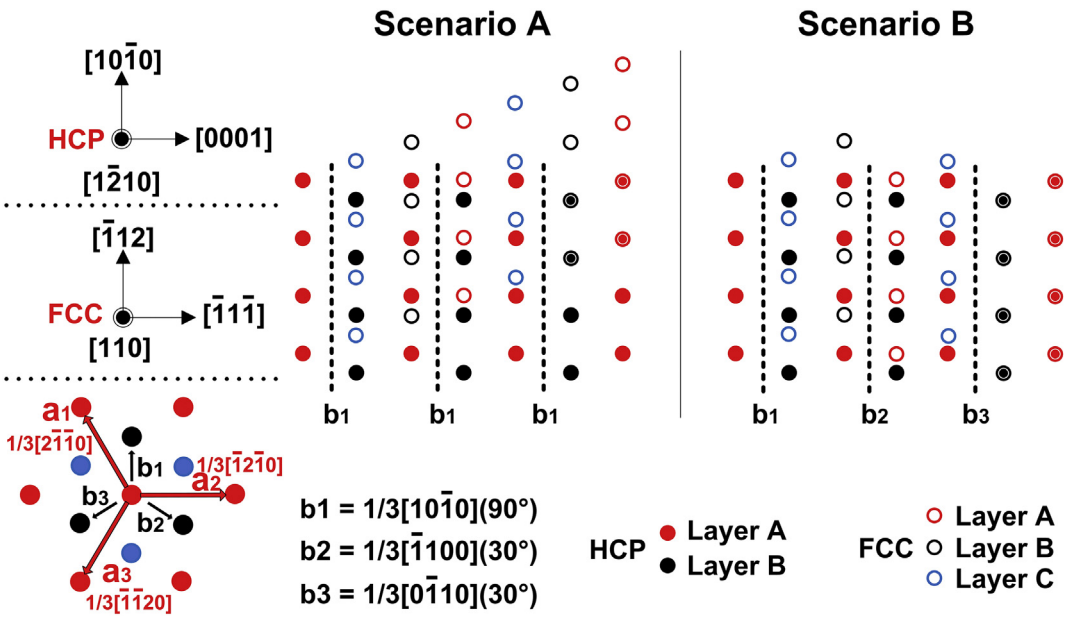

Fig. 3. Schematic illustration of the motion of atoms in Scenario A and Scenario B.

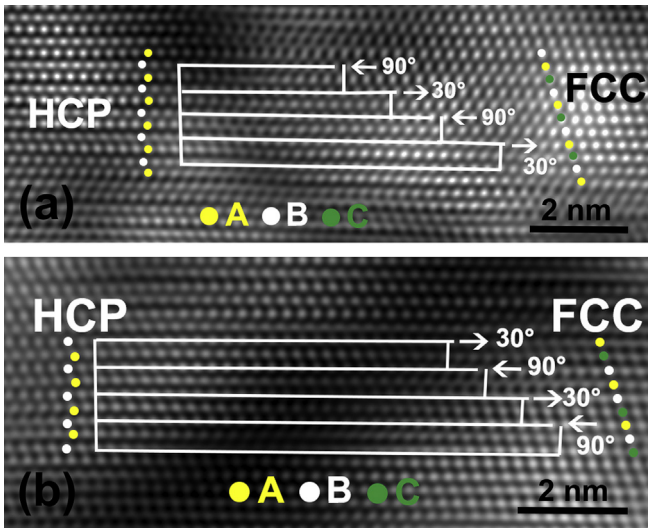

Fig. 4. (a) and (b) Two FFT-filtered high-resolution TEM images of HCP/FCC interfaces perpendicular to the basal plane, viewed from $[1\bar{2}10]_{hcp}//[110]_{fcc}$.

TEM experiments, the increase in the specimen temperature was only 12 K (see supplementary materials data S2). Such temperature rise has little effect on dislocation nucleation. For an Hf atom to be displaced to an interstitial position, energy of ~1200 keV is needed (see supplementary materials data S3). However, the electron beam energy in our experiments was only 300 keV, which is too low to produce any knock-on displacement. Therefore, both beam heating and knock-on displacement have negligible effects on the nucleation of partial dislocations in our experiments.

3.3. Density functional theory (DFT) calculation

In order to better understand the HCP to FCC phase transformation in Hf, the density functional theory (DFT) was used to analyze the formation of the FCC phase from the energy aspect, as shown in Fig. 7. The first principles density functional theory (DFT) calculations are carried out using the VASP code [42,43]. In our calculations, we used generalized gradient approximation (GGA) for the exchange correlation functional with the Perdew-Becke-Erzenh of (PBE) parameterization [44]. The interaction between valence electrons and ionic cores was treated using PAW pseudopotentials. It is suggested that for early transition metals (such as Hf), it is necessary to treat the semi core p states as valence [45]. Therefore, the numbers of valence electrons in the pseudopotentials are 10 ($5p^6$, $6s^2$, $5d^2$) for Hf. We used a plane wave energy cutoff of 275 eV, and optimized the atomic structure until the force on each atom is smaller than 0.02 eV/Å. The ground state of Hf adopts a hexagonal closed pack (HCP) structure. DFT calculations were performed for one hcp primitive unit cell with varying *a-c* combinations with step size $\Delta a = \Delta c = 0.001$ Å to find the optimized lattice parameters. In the calculations, we used a $12 \times 12 \times 8$ Γ-centered Monkhorst Packk-point mesh. The equilibrium lattice parameters for HCP-Hf are found to be a = 3.205 Å and c = 5.066 Å, giving c/a = 1.581, and −9.949 eV for the cohesive energy. These values are in good agreement with experimental measurements [46]. In the meantime, the FCC phase of Hf was also studied. We used a primitive unit cell of FCC structure and a $6 \times 6 \times 6$ MonkhorstPackk-point mesh. According to the fit of the Birch-Murnaghan equation of state, we found a = 4.478 Å for the lattice parameter, −9.876 eV for the cohesive energy and 102 GPa for the bulk modulus (Fig. 7(b)). It is evident that the cohesive energy of the FCC-Hf is higher than HCP-Hf by 0.073 eV, therefore HCP is the ground state of Hf.

To understand nucleation and growth of a FCC band in HCP Hf, we conducted the calculation of generalized stacking fault energy with respect to the shear across the habit planes in HCP and FCC structure. As shown in Fig. 7(c), the initial structure is a perfect HCP with stacking sequence: … ABABABAB …. When the half crystal is shifted along the black arrows (path 1), the low energy structure at |b| = 1 corresponds to … ABACBCBC …, containing a local FCC structure ACB. The transformation results an energy increase of 0.301 J/m^{2}and therefore energetically unfavorable. However, when a local FCC structure formed, an energy barrier 0.140 J/m^2 needs to be overcome in association with the recovery of HCP structure. When the half crystal is shifted along the red arrows(path 2), the

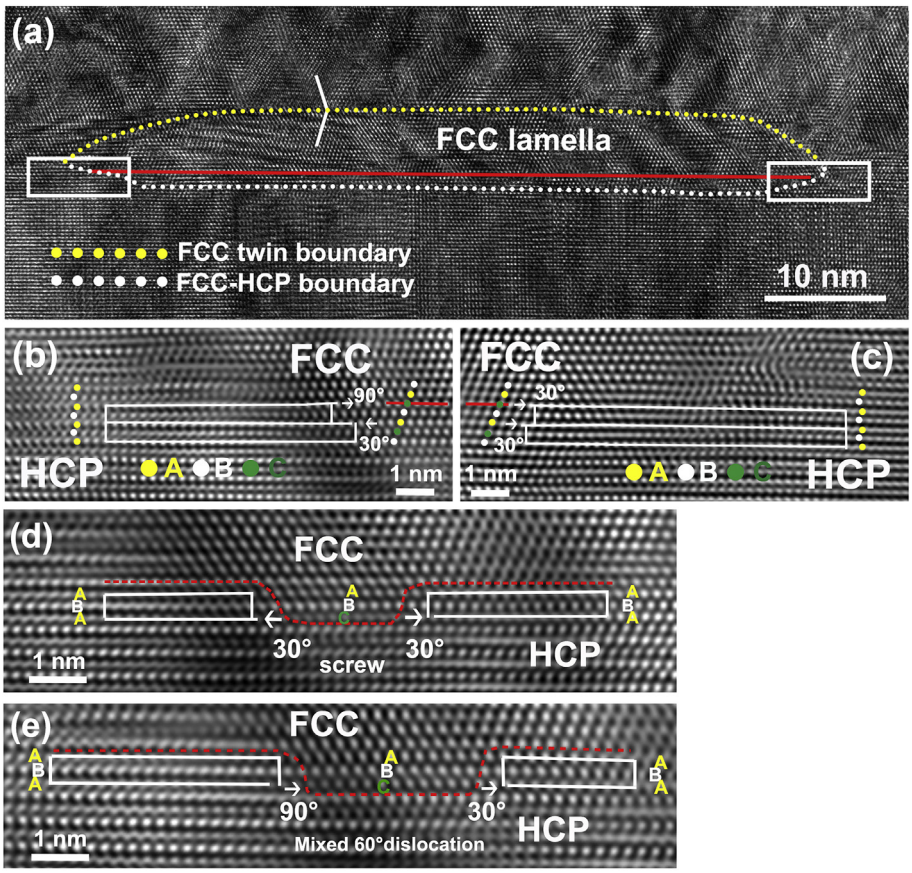

Fig. 5. (a) A high-resolution TEM image of a FCC lamella, projected along $<11\bar{2}0>_{hcp}//<110>_{fcc}$. (b) The FFT-filtered image of the left end of the FCC lamella. (c) the FFT-filtered image of the right end of the FCC lamella. (d) The dissociation of a 60° mixed dislocation. (e) The dissociation of a screw dislocation.

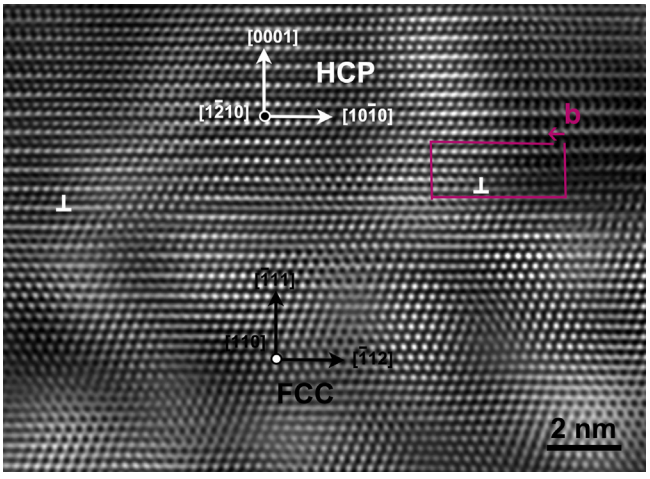

Fig. 6. An FFT-filtered high-resolution TEM image of the interface of HCP/FCC interface, projected along $<11\bar{2}0>_{HCP}//<110>_{FCC}$, the $\mathbf{b} = [112\ 0]_{HCP}$.

low energy structure at 2|b| is the same as the low energy structure … ABACBCBC …, while the metastable structure at |b| corresponds to … ABAABABA …, containing a high energy stacking fault structure AA, proving that path 1 is more favorable. Fig. 7(d) showed the inverse process. Through the DFT calculation, we concluded that the FCC structure is a metastable phase and has a higher cohesive energy (0.073eV/atom) than the HCP structure. The stacking fault energy (SFE) is 0.301 J/m^2 in HCP structure, but decreases to 0.210 J/m^2 in FCC structure. Such high SFE in HCP does not facilitate the nucleation and emission of partial dislocation. However, the SFE decreases in FCC structure once a FCC band nucleated. Thus, nucleation of a FCC band might be ascribed to a collective nucleation and propagation of partial dislocations. Since homogeneous nucleation of dislocation is difficult, one possible mechanism is the dissociation mechanism of full dislocations on the habit plane. Consequently, the dissociation of full dislocations happens on the FCC-HCP interface, growing the FCC band.

According to the crystallographic analysis, the HCP to FCC phase transformation leads to a lattice expansion normal to the <c> axis, which can effectively accommodate the macro-strain along the <c> axis. Accompanying with the transformation from HCP to FCC, a normal expansion perpendicular to the interface occurs (the interplanar spacing of $(0001)_{hcp} = 0.2533$ nm increases to the interplanar spacing of $(1\ 11)_{fcc} = 0.2585$ nm), corresponding to a transformation strain of 2.1%. This suggests that the transformation occurs when the HCP is subjected to an effective tension along the <c> axis. Once the FCC phase forms, it change the local stress due to the crystal expansion. As a result, FCC and HCP are subjected to compression. This compression strain reduces the tension strain in HCP and FCC domains. Thus HCP and FCC domains along the direction normal to the interface should have a smaller interplanar spacing from the experiment compared with DFT. Therefore, we measured the interplanar spacings of atomic plane (0002) in HCP-Hf and atomic plane$(1\ 11)$ in FCC-Hf as $d_{(0002)\ HCP} = 0.256\pm0.002$ nm and $d_{(\bar{1}11)FCC} = 0.271\pm0.003$ nm. However, compared with DFT data of zero-strain crystals: $d_{(0002)\ HCP} = 0.253$ nm; $d_{(\bar{1}11)FCC} = 0.259$ nm, we found that both the

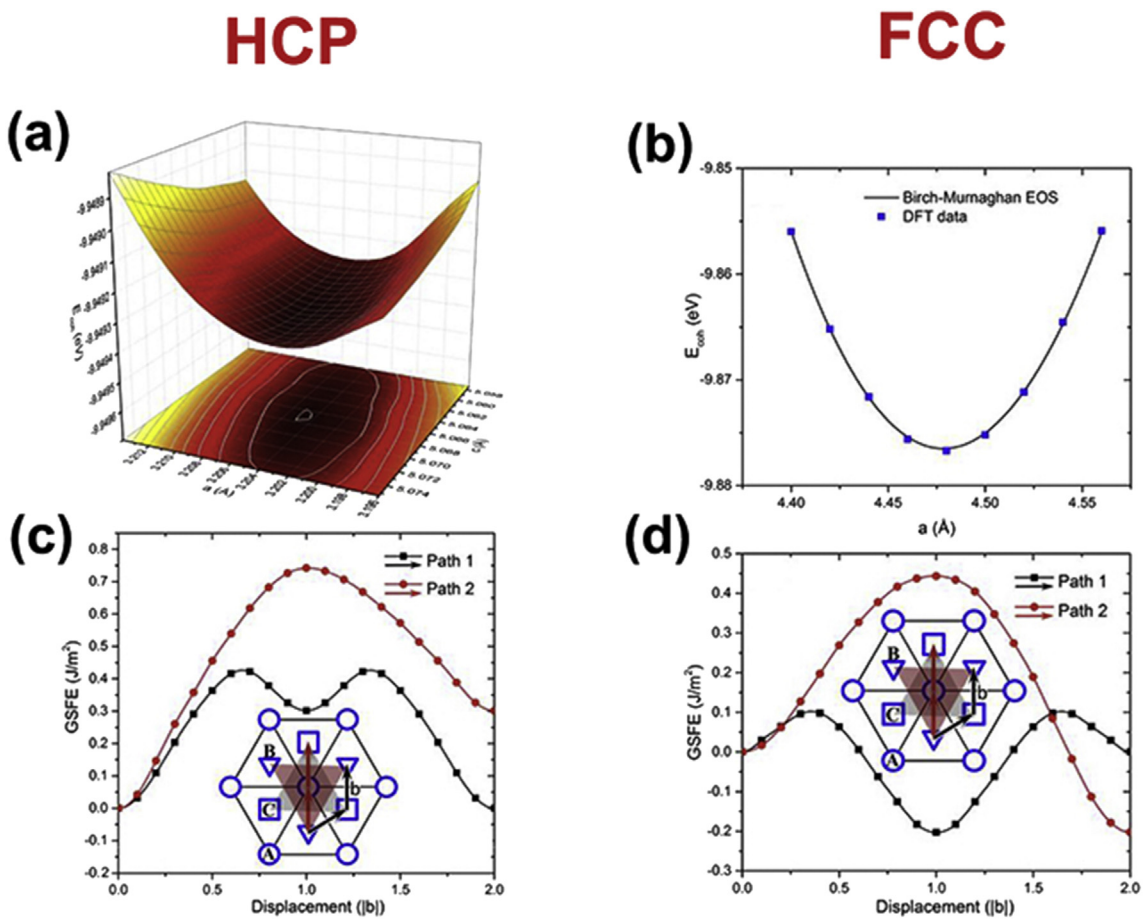

Fig. 7. Density Functional Calculation of Hafnium. (a) DFT calculations show that HCP-Hf has (1) lattice constants a = 0.3205 nm, c = 0.5066 nm, and c/a = 1.581, (2) cohesive energy = −9.949eV (lower than FCC). (b) DFT calculations show that FCC-Hf has (1) lattice constant = 0.4478 nm, (2) cohesive energy = −9.876eV. (c) The initial structure is a perfect HCP with stacking sequence: … ABABABAB …. When the half crystal is shifted along the black arrows, the low energy structure at |b| corresponds to … ABACBCBC …, containing a local FCC structure ACB. The transformation is energetically unfavored, resulting an energy increase of 0.301 J/m^2. When the half crystal is shifted along the red arrows, the low energy structure at 2|b| is the same as the low energy structure … ABACBCBC …, while the metastable structure at |b| corresponds to … ABAABABA …, containing a high energy stacking fault structure AA. (d) The initial structure is a perfect FCC with stacking sequence: … ABCABCABC …. When the half crystal is shifted along the black arrows, the low energy structure at |b| corresponds to … ABCACABCA …, containing a local HCP structure CACA. The transformation is energetically favored, resulting an energy drop of 0.210 J/m^2. When the half crystal is shifted along the red arrows, the low energy structure at 2|b| is the same as the low energy structure … ABCACABCA …, while the metastable structure at |b| corresponds to … ABCAABCAB …, containing a high energy stacking fault structure AA. (For interpretation of the references to colour in this figure legend, the reader is referred to the web version of this article.)

interplanar spacings are dilated, 1.19% in the HCP domain and 4.63% in the FCC domain, which means both domains still underwent a local tension along the direction normal to the interface after the phase transformation. It shows that the tension along the <c> axis not only triggered this phase transformation but also helped stabilize the FCC phase which is not a stable phase and must be stabilized under a hydrostatic expansion stress [23,47]. Previously research on the microstructural evolution of Hf during a rolling process showed that the activation of the <a>-type dislocation slip dominated the deformation [48], while twining and pyramidal slip which can accommodate the strain along <c> axis were hardly detected [48]. Nonetheless, that why the twins and pyramidal slip are suppressed while phase transformation is favored still needs investigation in the future.

3.4. The formation of twin relationship in FCC lamella

Twinning plays an important role in accommodating strain in FCC materials with low stacking fault energy [49,50]. Twins are frequently seen in FCC lamella in this study, as the FCC lamellas observed in Fig. 5(a). While some of the twins might form via the conventional deformation twinning mechanisms [49,50], we report here a new twinning mechanism. Fig. 8(a) shows numerous FCC lamellas dispersed in the HCP matrix and labels 1 and 2 represent two FCC lamellas. Their junction is circled by a yellow rectangular. Fig. 8(b) presents a high-resolution TEM image of the junction. It clearly shows that these two lamellas have a twin relationship with a wavy twin interface, which is marked by a white dotted line. The formation of this twin morphology is due to the difference in initial basal planes where the transformation-related partials extended. As the schematic illustration shown in Fig. 8(c), the HCP sequence is … ABABABA …. If the dislocation initially dissociated in … A|BABABA …, as shown in the left side of Fig. 8(c), the sequence would become … A|CBCBCB …. As remaining steps went on, the final FCC sequence would be … ABCABCA … (denoted as lamella 2). If the dislocation initially dissociated in … AB|ABABA …, as shown in the left side of Fig. 8(c), the final FCC sequence would be … ACBACBA … (denoted as lamella 1). These two sequences present a twin relationship. If FCC lamellas with different sequences encounter, they will merge into a larger FCC lamella. Based on schematic illustration in Fig. 8(c) and (d) shows how two FCC lamellas with different sequences encountered and merged. The red, black and blue dash

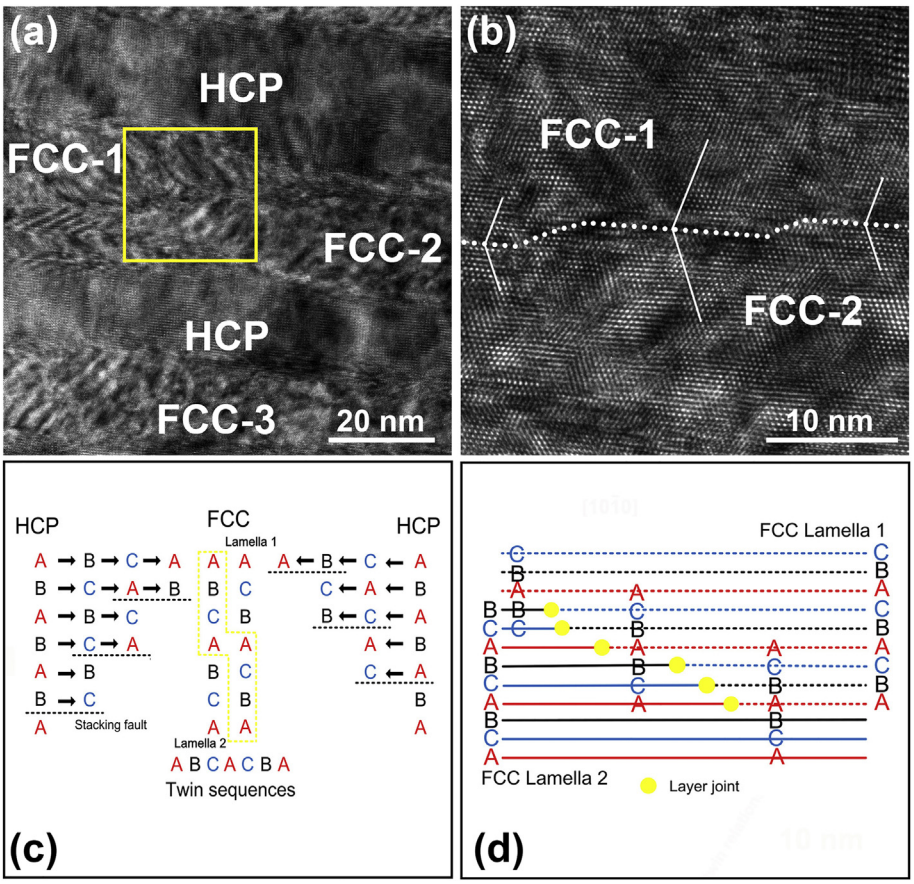

Fig. 8. (a) A bright-field image of the rolled specimen. Labels 1 and 2 indicate two FCC lamellas and their junction is marked by a yellow rectangular. (b) A high-resolution TEM image of the junction of two FCC lamellas marked in (a). (c)Schematic illustration of how the twin sequences form. (d) The encountering of two lamellas and formed a twin relationship: dash lines represent layers in FCC lamella 1, while solid lines represent layers in FCC lamella 2. The layer joints are indicated by yellow dots. (For interpretation of the references to colour in this figure legend, the reader is referred to the web version of this article.)

line represent layer A, B and C in FCC lamella 1, respectively. The red, black and blue solid line represent layer A, B and C in FCC lamella 2, respectively. As the transformation-involved partials in FCC lamella 1 and FCC lamella 2 moved toward left and right respectively, layers in lamellas 1 and 2 would encounter and form layer joints. The connection line of these layer joints is the boundary of lamellas 1 and 2. Thus, a twinning relationship formed. It is worth mentioning that such phenomenon is easily seen in the TEM specimen. The growth of FCC lamella can also be realized by the merging of small lamella with the same orientation or with twin relationship (an example is shown in Supplemental Material Fig. S4). One possible reason for the formation of the twin structure is, if an FCC band results in a shear strain (no matter small or big), and another FCC band can result in an opposite shear strain, then the domain containing the two FCC bands will result in a small strain in the matrix. Such mechanical advantage will favor twin formation.

4. Conclusion

A stress-induced transformation from the HCP phase to the FCC phase occurred in Hf during a cold-rolling process. The FCC phase appeared in the form of lamellar grains with a width of up to ~50 nm. Atomic-resolution TEM image analysis suggests that the phase transformation was triggered by Shockley partial dislocations with Burgers vector $1/3<01\bar{1}0>$ gliding on the basal plane. These transformation-related partials were randomly displayed at the tips of FCC lamellas with different Burgers vectors. These partials stemmed from the dissociation of <a>-type dislocations. Besides the effect of partial dislocations, the growth of FCC lamella can also be realized by merging small lamella with the same orientation or with a twin relationship.

Acknowledgements

The financial supports from National Natural Science Foundation of China (51301207), Fundamental Research Funds for the Central Universities of Central South University (2016zzts264), are appreciated. Wang acknowledges financial support provided by the Nebraska Center for Energy Sciences Research at the University of Nebraska-Lincoln. Liao and Song thank Australian Research Council for financial support (DP150101121). Shao acknowledges the start-up support provided by the Louisiana State University.

Appendix A. Supplementary data

Supplementary data related to this article can be found at http://dx.doi.org/10.1016/j.actamat.2017.03.058.

References

[1] X.S. Yang, S. Sun, T.Y. Zhang, The mechanism of bcc α' nucleation in single hcp ε laths in the fcc γ→hcp ε→bcc α' martensitic phase transformation, Acta Mater. 95 (2015) 264–273.
[2] X.S. Yang, S. Sun, X.L. Wu, E. Ma, T.Y. Zhang, Dissecting the mechanism of

martensitic transformation via atomic-scale observations, Sci. Rep. 4 (2014) 6141.
[3] M. Ekman, B. Sadigh, K. Einarsdotter, Ab initio study of the martensitic bcc-hcp transformation in iron, Phys. Rev. B 58 (1998) 5296–5304.
[4] A. Ojha, S. Sehitoglu, Critical stress for the bcc–hcp martensite nucleation in Ti–6.25at.%Ta and Ti–6.25at.%Nb alloys, Comput. Mater. Sci. 111 (2016) 157–162.
[5] S.R. Nishitani, H. Kawabe, M. Aoki, First-principles calculations on bcc–hcp transition of titanium, Mater. Sci. Eng. A 312 (2001) 77–83.
[6] X. Wu, N. Tao, Y. Hong, G. Liu, B. Xu, J. Lu, K. Lu, Strain-induced grain refinement of cobalt during surface mechanical attrition treatment, Acta Mater. 53 (2005) 681–691.
[7] G.P. Zheng, Y.M. Wang, M. Li, Atomistic simulation studies on deformation mechanism of nanocrystalline cobalt, Acta Mater. 53 (2005) 3893–3901.
[8] T. Waitz, H.P. Karnthaler, The f.c.c. to h.c.p. martensitic phase transformation in CoNi studied by TEM and AFM methods, Acta Mater. 45 (1997) 837–847.
[9] Y.N. Liu, H. Yang, T. Geraldine, M. Shuichi, B.H. Jiang, Y. Liu, Stress-induced FCC↔HCP martensitic transformation in CoNi, J. Alloys Compd. 368 (2004) 157–163.
[10] D.H. Hong, T.W. Lee, S.H. Lim, W.Y. Kim, S.K. Hwang, Stress-induced hexagonal close-packed to face-centered cubic phase transformation in commercial-purity titanium under cryogenic plane-strain compression, Scr. Mater. 69 (2013) 405–408.
[11] H.C. Wu, A. Kumar, J. Wang, X.F. Bi, C.N. Tomé, Z. Zhang, S.X. Mao, Rolling-induced face centered cubic titanium in hexagonal close packed titanium at room temperature, Sci. Rep. 6 (2016) 24370.
[12] R. Jing, C.Y. Liu, M.Z. Ma, R.P. Liu, Microstructural evolution and formation mechanism of FCC titanium during heat treatment processing, J. Alloys Compd. 552 (2013) 202–207.
[13] R. Jing, S.X. Liang, C.Y. Liu, M.Z. Ma, R.P. Liu, Aging effects on the microstructures and mechanical properties of the Ti–20Zr–6.5Al–4V alloy, Mater. Sci. Eng. A 559 (2013) 474–579.
[14] Y. Koizumi, T. Fujita, Y. Minamino, S. Hata, Effects of plastic deformation on lamellar structure formation in Ti–39at.% Al single crystals, Acta Mater. 58 (2010) 1104–1114.
[15] H. Zheng, J. Wang, J.Y. Huang, J.B. Wang, Z. Zhang, S.X. Mao, Dynamic process of phase transition from wurtzite to zinc blende structure in InAs nanowires, Nano Lett. 13 (2013) 6023–6027.
[16] U.M.R. Seelam, C. Suryanarayana, Mechanically induced fcc phase formation in nanocrystalline hafnium, J. Appl. Phys. 105 (2009) 063524.
[17] O. Levy, L.W. Hart, S. Curtarolo, Hafnium binary alloys from experiments and first principles, Acta Mater. 58 (2010) 2887–2897.
[18] G.D. Wilk, R.M. Wallace, J.M. Anthony, High-κ gate dielectrics: current status and materials properties considerations, J. Appl. Phys. 89 (2001) 5243–5275.
[19] V.D. Risovany, V.I. Prokhorov, Z.E. Ostrovsky, V.V. Pimenov, A.V. Zakharov, E.M. Muraleva, Structure and properties of hafnium after a 9-year operation in the RBT-6 research reactor, J. Nucl. Mater. 402 (2010) 157–161.
[20] Y.K. Vohra, Kinetics of phase transformations in Ti, Zr and Hf under static and dynamic pressures, J. Nucl. Mater. 75 (1978) 288–294.
[21] S.K. Sikka, Y.K. Vohra, R. Chidambaram, Omega phase in materials, Prog. Mater. Sci. 27 (1982) 245–310.
[22] H. Xia, G. Parthasarathy, H. Luo, Y.K. Vohra, A.L. Ruoff, Crystal structures of group IVa metals at ultrahigh pressures, Phys. Rev. B 42 (1990) 6736–6738.
[23] H.L. Zhao, S. Ni, M. Song, Mechanically induced phase transformation from hexagonal close packed structure to face-centred cubic structure in hafnium, Mater. Sci. Eng. A 660 (2016) 34–38.
[24] X.Z. Liao, F. Zhou, E.J. Lavernia, D.W. He, Y.T. Zhu, Deformation twins in nanocrystalline Al, Appl. Phys. Lett. 83 (2003) 5062–5064.
[25] X.Z. Liao, F. Zhou, E.J. Lavernia, S.G. Srinivasan, M.I. Baskes, D.W. He, Y.T. Zhu, Deformation twinning in nanocrystalline copper at room temperature and low strain rate, Appl. Phys. Lett. 84 (2003) 592–594.
[26] V. Yamakov, D. Wolf, S.R. Phillpot, A.K. Mukherjee, H. Gleiter, Dislocation processes in the deformation of nanocrystalline aluminium by molecular-dynamics simulation, Nat. Mater. 1 (2002) 45–48.
[27] X.L. Wu, X.Z. Liao, S.G. Srinivasan, F. Zhou, E.J. Lavernia, R.Z. Valiev, Y.T. Zhu, New deformation twinning mechanism generates zero macroscopic strain in nanocrystalline metals, Phys. Rev. Lett. 100 (2008) 095701.
[28] J. Wang, N. Li, O. Anderoglu, X. Zhang, A. Misra, J.Y. Huang, J.P. Hirth, Detwinning mechanisms for growth twins in face-centered cubic metals, Acta Mater. 58 (2010) 2262–2270.
[29] A.Y. Clarissa, K.C. Ellen, G.T. Gray, W.B. Donald, C.V. Sven, The effect of twinning on the work-hardening behavior and microstructural evolution of hafnium, Metall. Mater. Trans. A 37A (2006) 1907–1915.
[30] E. Cerreta, G.T. Gray, The influence of texture, strain rate, temperature, and chemistry on the mechanical behavior of hafnium, Metall. Mater. Trans. A 35A (2004) 1999–2011.
[31] L. Wang, Z. Zhang, X. Han, In situ experimental mechanics of nanomaterials at the atomic scale, NPG Asia Mater. 5 (2013) e40.
[32] E. Bitzek, P. Gumbsch, Mechanisms of dislocation multiplication at crack tips, Acta Mater. 61 (2013) 1394–1403.
[33] T. Shimokawa, M. Tsuboi, Atomic-scale intergranular crack-tip plasticity in tilt grain boundaries acting as an effective dislocation source, Acta Mater. 87 (2015) 233–247.
[34] Z.H. Jin, P. Gumbsch, E. Ma, K. Albe, K. Lu, H. Hahn, H. Gleiter, The interaction mechanism of screw dislocations with coherent twin boundaries in different face-centred cubic metals, Acta Mater. 54 (2006) 1163–1168.
[35] Z.H. Jin, P. Gumbsch, E. Ma, K. Albe, K. Lu, H. Hahn, H. Gleiter, Interactions between non-screw lattice dislocations and coherent twin boundaries in face-centered cubic metals, Acta Mater. 56 (2008) 1126–1135.
[36] L.H. Wang, P. Liu, P.F. Guan, M.J. Yang, J.L. Sun, Y.Q. Cheng, A. Hirata, Z. Zhang, E. Ma, M.W. Chen, X.D. Han, In situ atomic-scale observation of continuous and reversible lattice deformation beyond the elastic limit, Nat. Commun. 4 (2013) 2413.
[37] D.J. Bacon, V. Vitek, atomic-scale modeling of dislocations and related properties in the hexagonal-close-packed metals, Metall. Mater. Trans. A 33A (2002) 721–733.
[38] D.H. Kim, F. Ebrahimi, M.V. Manuel, J.S. Tulenko, S.R. Phillpot, Grain-boundary activated pyramidal dislocations in nano-textured Mg by molecular dynamics simulation, Mater. Sci. Eng. A 528 (2011) 5411–5420.
[39] Y.Z. Tang, A. Jaafar, El-Awady, Formation and slip of pyramidal dislocations in hexagonal close-packed magnesium single crystals, Acta Mater. 71 (2014) 319–332.
[40] L.H. Wang, K. Zheng, Z. Zhang, X.D. Han, Direct atomic-scale imaging about the mechanisms of ultralarge bent straining in Si nanowires, Nano Lett. 11 (2011) 2382–2385.
[41] K. Zheng, C.K. Wang, Y.Q. Cheng, Y.H. Yue, X.D. Han, Z. Zheng, Z.W. Shan, S.X. Mao, M.M. Ye, Y.D. Yin, E. Ma, Electron-beam-assisted superplastic shaping of nanoscale amorphous silica, Nat. Commun. 1 (2010) 24.
[42] G. Kresse, J. Hafner, Ab initio molecular dynamics for open-shell transition metals, Phys. Rev. B 48 (1993) 13115.
[43] G. Kresse, W.J. Furthmut, Efficient iterative schemes for ab initio total-energy calculations using a plane-wave basis set, Phys. Rev. B 54 (1996) 11169.
[44] J.P. Perdew, K. Burke, M. Ernzerhof, Generalized gradient approximation made simple, Phys. Rev. Lett. 77 (1996) 3865–3868.
[45] G. Kresse, D. Joubert, From ultrasoft pseudopotentials to the projector augmented-wave method, Phys. Rev. B 59 (1999) 1758–1775.
[46] D.R. Lide, CRC Handbook of Chemistry and Physics, CRC Press, New York, 2010.
[47] S.Y. Xiong, W.H. Qi, B.Y. Huang, M.P. Wang, L.Y. Wei, Gibbs free energy and size–temperature phase diagram of hafnium nanoparticles, J. Phys. Chem. C 115 (2011) 10365–10369.
[48] H.L. Zhao, S. Ni, M. Song, X. Xiong, X.P. Liang, H.Z. Li, Grain refinement via formation and subdivision of microbands and thin laths structures in cold-rolled hafnium, Mater. Sci. Eng. A 645 (2015) 328–332.
[49] Y.T. Zhu, X.Z. Liao, X.L. Wu, Deformation twinning in nanocrystalline materials, Prog. Mater. Sci. 57 (2012) 1–62.
[50] J.W. Christian, S. Mahajan, Deformation twinning, Prog. Mater. Sci. 39 (1995) 1–157.